PERGAMON

International Journal of Heat and Mass Transfer 45 (2002) 2265–2276

International Journal of HEAT and MASS TRANSFER

www.elsevier.com/locate/ijhmt

Inertia effects on non-parallel thermal instability of natural convection flow over horizontal and inclined plates in porous media

J.Z. Zhao, T.S. Chen *

Department of Mechanical and Aerospace Engineering and Engineering Mechanics, University of Missouri-Rolla, Rolla, MO 65409, USA

Received 23 May 2001; received in revised form 18 October 2001

Abstract

The inertia effect on the onset of thermal instability in natural convection flow over heated horizontal and inclined flat plates embedded in fluid-saturated porous media is analyzed. The linear non-parallel flow model is employed in the instability analysis, which takes into account the streamwise variation as well as the transverse variation of the disturbance amplitude functions. The set of partial differential equations for the disturbance amplitude functions are converted to a system of homogeneous linear ordinary differential equations with homogeneous boundary conditions by the local non-similarity method. The resulting eigenvalue problem is then solved by an implicit finite-difference method. Representative neutral stability curves and critical Rayleigh numbers are presented. It has been found that as the angle of inclination relative to the horizontal increases, the surface heat transfer rate increases, whereas the flow becomes more stable to the vortex mode of instability. Also, as the inertia effect, expressed in terms of Forchheimer number, *Fr*, increases, the heat transfer rate decreases, but the flow becomes more stable. It is demonstrated that the non-parallel flow model predicts a more stable flow than the parallel flow model.

1. Introduction

It is well known that a secondary flow in the form of longitudinal vortex rolls can occur in natural convection over a heated horizontal or inclined plate due to the presence of a buoyancy force component normal to the plate surface [1,2]. Extensive theoretical studies on the onset of longitudinal vortex rolls in natural convection for clear fluids have been conducted by many investigators (see, for example [3–6]) using the standard linear theory in conjunction with a parallel flow model which neglects the streamwise dependence of the disturbance amplitude functions. Later studies conducted by Lee et al. [7–10] have shown that the stability characteristics change significantly when the non-parallel flow model is applied to the disturbance flow, wherein the amplitude functions of the disturbances depend on both the streamwise and transverse coordinates.

The study on the vortex instability of laminar boundary layer flow in porous media has received considerable attention since the work of Hsu et al. [11] on natural convection flow over a horizontal flat plate. Their analysis was based on a linear quasi-parallel flow model and the disturbance amplitude equations were solved by the similarity method. Subsequently, Hsu and Cheng [12,13] studied the vortex instability of natural convection flow and mixed convection flow along inclined flat plates. In these studies, the similarity solutions for a vertical plate were used as an approximation to the basic flow for the inclined plate, and the vortex instability was then analyzed using a non-parallel flow model, but the solutions were carried out by the local similarity method. Later, Jang and Chang [14,15] re-examined the works of Hsu and Cheng [12,13] using a more accurate basic flow solutions.

* Corresponding author. Tel.: +1-573-341-4628; fax: +1-573-341-4607.

E-mail address: tschen@umr.edu (T.S. Chen).

0017-9310/02/$ - see front matter
PII: S0017-9310(01)00320-9

Nomenclature

a	spanwise wave number of the vortex roll
c	inertia coefficient
D	partial derivative with respect to η
Da_x	local Darcy number, K/x^2
f	dimensionless stream function
Fr	Forchheimer number, $5^{(1-m)}c^{(2-m)}g\beta AK^{5/2}\alpha^{(1-m)}/\nu^{(3-m)}$
g	gravitational acceleration
h	convective heat transfer coefficient, $-k(\partial\bar{T}/\partial y)_{y=0}/[T_w(x)-T_\infty]$
k	thermal conductivity of porous medium, or dimensionless wave number, $ax/(Ra_x/5)^{1/5}$
K	Darcy permeability
m	exponent in the wall temperature variation
Nu_x	local Nusselt number, hx/k
p	pressure
Pr	Prandtl number
Ra_x	local Rayleigh number, $g\beta x^3[T_w(x)-T_\infty]/(\nu\alpha)$
t	time
T	temperature
u, v, w	streamwise, normal, and spanwise velocity components in the x, y, z directions
x, y, z	streamwise, normal and spanwise coordinates

Greek symbols

α	effective thermal diffusivity
β	coefficient of thermal expansion
γ	spatial growth of the vortex roll, $\int \alpha_i(x)\mathrm{d}x$, with α_i denoting the spatial growth factor
η	pseudo-similarity variable, $(y/x)(Ra_x/5)^{1/5}$
θ	dimensionless temperature
λ	volumetric heat capacity of the saturated porous medium to that of the fluid
μ	fluid dynamic viscosity
ν	fluid kinematic viscosity
ξ	non-similarity parameter, $1/[Da_x(Ra_x/5)^{2/5}]$
ρ	fluid density
σ	temporal growth factor of the vortex roll
φ	inclination angle from the horizontal
ψ	stream function

Superscripts

$-$	basic flow quantities
$'$	infinitesimal disturbance quantities
$+$	dimensionless quantities for disturbance flow
$\sim$	amplitude of disturbance quantities
$*$	critical parameters

Subscripts

w	condition at the wall
∞	condition at the free stream

The representative investigations on thermal instability mentioned above are for Darcy flow and are based on the quasi-parallel flow model. However, with high flow rates or high permeability in porous media, there is a departure from Darcy's law and the inertia effect, which is caused by the form drag due to the solid matrix, becomes significant. The inertia effect on vortex instability of natural convection flow in a porous medium was first examined by Chang and Jang [16] for flow over a horizontal flat plate. Their results showed that the inertia effect has a destabilizing effect on the flow. However, their interpretation of the inertia term in the momentum equations for the Forchheimer model was questioned by Lee et al. [17] who corrected the Forchheimer term as used by Chang and Jang [16] and examined the inertia effect as well as the thermal dispersion effect on the vortex instability of natural convection flow over an inclined plate. Contrary to the findings of Chang and Jang [16], their results showed that the inertia effect has a stabilizing effect on the flow. In the study of Lee et al. [17], the basic flow solutions were obtained using an approximate similarity solution for a vertical plate by incorporating the gravity component parallel to the inclined plate in the Rayleigh number and neglecting the normal buoyancy force component that induces the streamwise pressure gradient in the flow. Therefore, their basic flow and instability results are expected to be valid only for small angles of inclination from the vertical. The normal buoyancy force component plays an important role in the onset of the vortex instability when the angles of inclination from the vertical (horizontal) are relatively large (small). In addition, no fully reliable analyses seem to exist for the vortex instability of natural convection flow over a horizontal plate in porous media with significant inertia effects.

In the vortex instability analyses of natural convective flow, the previous investigators have employed the quasi-parallel flow model, which assumes a weak dependence of the disturbance amplitude functions on the streamwise coordinate or the non-similarity parameter $\xi(x)$ (i.e., $\partial/\partial\xi << \partial/\partial\eta$), in their numerical solutions. This assumption is not consistent with the non-parallel flow model where the disturbance amplitude functions are taken to depend on both the x and y coordinates. The studies conducted by Lee et al. [7–10] on thermal instability of clear fluid flows have shown that big differences in the results exist between the parallel and non-parallel flow models. In addition, when compared with available experimental data, the non-parallel flow model has been found to provide more accurate results than the parallel flow model.

A survey of literature has revealed that most of the past studies on vortex instability of natural convection flow in porous media are inadequate. To the authors' best knowledge, no vortex instability analyses exist for flow in a porous medium, that employ the fully non-parallel flow model in which both the x and y dependence of the disturbance amplitude functions are considered. This has motivated the present study to re-examine the inertia effect on the vortex instability of natural convection flow over horizontal and inclined flat plates embedded in a fluid-saturated porous medium by employing the non-parallel flow model. Such an analysis will lead to a system of non-similar equations for the disturbance amplitude functions. In the basic flow, the boundary layer approximations are invoked and the resulting governing equations are transformed into a system of non-similar dimensionless equations that are then solved by an implicit finite-difference method. The stability analysis is based on the linear non-parallel flow model. The resulting governing equations for the disturbance amplitude functions are partial differential equations that are converted into a system of homogeneous linear ordinary differential equations with homogeneous boundary conditions by the local similarity method. The resulting eigenvalue problem is then solved by an implicit finite-difference method.

It is noted here that, as the inertia effect becomes significant, thermal dispersion will play a role in altering the temperature profile, which in turn would affect the thermal instability results. In the present study, the thermal dispersion effect is neglected in the analysis for simplicity, because the major aim is to compare the thermal instability results between the non-parallel flow model and the parallel flow model. However, the inclusion of thermal dispersion effects on thermal instability would be an appropriate topic for future study.

2. Analysis

The physical system considered is a semi-infinite, inclined flat plate embedded in a porous medium, as shown in Fig. 1. The plate is inclined from the horizontal plane with an acute angle φ. The x-axis is taken along the plate in the flow direction, the y-axis is perpendicular to the plate and points outward into the porous medium, and the z-axis is in the spanwise direction across the plate. The ambient temperature of the porous medium is uniform at T_∞ and the wall temperature is kept at a higher value with the power-law variation, $T_w(x) = T_\infty + Ax^m$, where A and m are constants. To simplify the analysis, the following conventional assumptions are applied: (1) the fluid and the porous solid matrix are in local thermodynamic equilibrium; (2) the porous medium is everywhere isotropic and homogeneous; (3) the fluid properties are constant except for the density in the buoyancy force term; (4) the Boussinesq approximation is employed; and (5) the Forchheimer non-Darcy model is used for high flow rates or high permeability in the porous medium. The conservation equations are

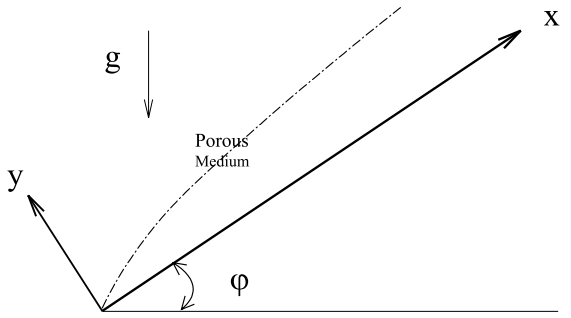

Fig. 1. Schematic diagram of the flow configuration.

$$\nabla \cdot \vec{u} = 0, \tag{1}$$

$$\frac{\mu}{K}\vec{u} + \rho_\infty c|\vec{u}|\vec{u} = -\nabla p - \rho\vec{g}, \tag{2}$$

$$\lambda\frac{\partial T}{\partial t} + \vec{u}\cdot\nabla T = \alpha\nabla^2 T, \tag{3}$$

where K and c are, respectively, the permeability and the inertia coefficient of the porous medium; the arrow bar over a symbol represents a vector variable; α is the effective thermal diffusivity of the medium, and p is the pressure. The other symbols are defined in the nomenclature.

2.1. The basic flow

The conservation equations, Eqs. (1)–(3), for the steady two-dimensional laminar flow along an inclined flat plate can be written as

$$\frac{\partial \bar{u}}{\partial x} + \frac{\partial \bar{v}}{\partial y} = 0, \tag{4}$$

$$\frac{\mu}{K}\bar{u} + \rho_\infty c|\vec{u}|\bar{u} = -\frac{\partial \bar{p}}{\partial x} - \rho g\cdot\sin\varphi, \tag{5}$$

$$\frac{\mu}{K}\bar{v} + \rho_\infty c|\vec{u}|\bar{v} = -\frac{\partial \bar{p}}{\partial y} - \rho g\cdot\cos\varphi, \tag{6}$$

$$\bar{u}\frac{\partial \bar{T}}{\partial x} + \bar{v}\frac{\partial \bar{T}}{\partial y} = \alpha\left(\frac{\partial^2 \bar{T}}{\partial x^2} + \frac{\partial^2 \bar{T}}{\partial y^2}\right), \tag{7}$$

with the Boussinesq approximation

$$\rho = \rho_\infty[1 - \beta(\bar{T} - T_\infty)]. \tag{8}$$

The pressure terms appearing in Eqs. (5) and (6) can be eliminated through cross-differentiation and subtraction. By applying the boundary layer assumptions and introducing the stream function ψ, which automatically satisfies the mass conservation Eq. (4) with $\bar{u} = \partial\psi/\partial y$

and $\bar{v} = -\partial\psi/\partial x$, the above governing equations can be reduced to

$$\left(1 + \frac{2Kc}{\nu}\cdot\frac{\partial\psi}{\partial y}\right)\frac{\partial^2\psi}{\partial y^2} = \frac{\rho_\infty g\beta K}{\mu}\left(\frac{\partial\bar{T}}{\partial y}\sin\varphi - \frac{\partial\bar{T}}{\partial x}\cos\varphi\right), \tag{9}$$

$$\frac{\partial\psi}{\partial y}\frac{\partial\bar{T}}{\partial x} - \frac{\partial\psi}{\partial x}\frac{\partial\bar{T}}{\partial y} = \alpha\frac{\partial^2\bar{T}}{\partial y^2}. \tag{10}$$

It is noted that, with the boundary layer assumption, the term $|\vec{u}|$ in Eqs. (5) and (6) can be approximated as $|\vec{u}| = \sqrt{\bar{u}^2 + \bar{v}^2} \approx |\bar{u}| = \bar{u}$ based on the fact that there is no recirculation region in laminar flow. The corresponding boundary conditions are

$$\begin{aligned} &y = 0: \quad \bar{v} = 0 \text{ or } \partial\psi/\partial x = 0, \quad T_w = T_\infty + Ax^m,\\ &y \to \infty: \quad \bar{u} = 0 \text{ or } \partial\psi/\partial y = 0, \quad \bar{T} = T_\infty. \end{aligned} \tag{11}$$

To transform Eqs. (9)–(11) into a dimensionless form, the following variables are introduced

$$\eta(x,y) = \frac{y}{x}(Ra_x/5)^{1/5}, \quad \xi(x) = \frac{1}{Da_x(Ra_x/5)^{2/5}},$$

$$f(\xi,\eta) = \frac{\psi(x,y)}{5\alpha(Ra_x/5)^{1/5}}, \quad \theta(\xi,\eta) = \frac{\bar{T} - T_\infty}{T_w - T_\infty}, \tag{12}$$

where $Ra_x = g\beta x^3(T_w - T_\infty)/\nu\alpha$ is the local Rayleigh number and $Da_x = K/x^2$ is the local Darcy number. The transformation of Eqs. (9)–(11) from the (x,y) to the (ξ,η) coordinates yields the following system of equations

$$\begin{aligned} &\xi f'' + 2Fr^{1/(2-m)}\xi^{5/(4-2m)}f'f'' - (Ra_x/5)^{1/5}\theta'\cdot\sin\varphi\\ &\quad + \left(m\theta + \frac{m-2}{5}\eta\theta' + \frac{4-2m}{5}\xi\frac{\partial\theta}{\partial\xi}\right)\cdot\cos\varphi = 0, \end{aligned} \tag{13}$$

$$\theta'' + (m+3)f\theta' - 5mf'\theta = (4-2m)\xi\left(f'\frac{\partial\theta}{\partial\xi} - \theta'\frac{\partial f}{\partial\xi}\right), \tag{14}$$

with the boundary conditions

$$\begin{aligned} &\eta = 0: \quad f(\xi,0) + \frac{\partial f(\xi,0)}{\partial\xi} = 0 \text{ or } f(\xi,0) = 0,\\ &\qquad \theta(\xi,0) = 1,\\ &\eta \to \infty: \quad f'(\xi,\infty) = 0, \quad \theta(\xi,\infty) = 0. \end{aligned} \tag{15}$$

In Eqs. (13)–(15) the primes denote partial differentiation with respect to η. The parameter

$$Fr = 5^{(1-m)}c^{(2-m)}g\beta AK^{5/2}\alpha^{(1-m)}/\nu^{(3-m)}$$

is the Forchheimer number expressing the relative importance of the inertia effect. The non-similarity parameter ξ characterizes the local strength of the buoyancy-induced flow (Ra_x) and the permeability (K) of the porous medium. As x increases or ΔT and K decrease, the value of $\xi(x)$ increases. It is noted that Darcy's law corresponds to the case of $\xi \to \infty$ (i.e., $K \to 0$) and $Fr = 0$.

In terms of the new transformation variables ξ and η, the streamwise and transverse velocity components and the local Nusselt number are given by the expressions

$$\begin{aligned} &\bar{u} = \frac{5\alpha}{x}(Ra_x/5)^{2/5}f',\\ &\bar{v} = -\frac{\alpha}{x}(Ra_x/5)^{1/5}\left[(m+3)f + (4-2m)\xi\frac{\partial f}{\partial\xi} + (m-2)\eta f'\right],\\ &Nu_x(Ra_x/5)^{-1/5} = -\theta'(\xi,0). \end{aligned} \tag{16}$$

2.2. The disturbance flow

The linear non-parallel flow theory is employed in the instability analysis, in which the temperature, pressure, and velocity distributions are decomposed into the basic undisturbed quantities and the infinitesimal disturbance quantities as

$$\begin{aligned} T(x,y,z,t) &= \bar{T}(x,y) + T'(x,y,z,t),\\ p(x,y,z,t) &= \bar{p}(x,y) + p'(x,y,z,t),\\ u(x,y,z,t) &= \bar{u}(x,y) + u'(x,y,z,t),\\ v(x,y,z,t) &= \bar{v}(x,y) + v'(x,y,z,t),\\ w(x,y,z,t) &= w'(x,y,z,t), \end{aligned} \tag{17}$$

where the barred and primed quantities designate, respectively, the undisturbed basic flow and the disturbance flow components. It is assumed that the basic flow is a steady, two-dimensional, buoyancy-induced boundary-layer flow whose solution is governed by Eqs. (9)–(11) or Eqs. (13)–(15). The disturbance flow is three-dimensional.

Substituting Eq. (17) into Eqs. (1)–(3), subtracting the basic flow quantities and linearizing the equations by neglecting terms higher than the first order in the disturbance quantities, one can arrive at the following equations for the disturbances

$$\frac{\partial u'}{\partial x} + \frac{\partial v'}{\partial y} + \frac{\partial w'}{\partial z} = 0, \tag{18}$$

$$\frac{\mu}{K}u' + \rho_\infty c\left|\vec{u}\right|u' = -\left[\frac{\partial p'}{\partial x} - \rho_\infty\beta gT'\sin\varphi\right], \tag{19}$$

$$\frac{\mu}{K}v' + \rho_\infty c\left|\vec{u}\right|v' = -\left[\frac{\partial p'}{\partial y} - \rho_\infty\beta gT'\cos\varphi\right], \tag{20}$$

$$\frac{\mu}{K}w' + \rho_\infty c\left|\vec{u}\right|w' = -\left[\frac{\partial p'}{\partial z}\right], \tag{21}$$

$$\begin{aligned} &\lambda\frac{\partial T'}{\partial t} + \bar{u}\frac{\partial T'}{\partial x} + u'\frac{\partial\bar{T}}{\partial x} + \bar{v}\frac{\partial T'}{\partial y} + v'\frac{\partial\bar{T}}{\partial y}\\ &\quad = \alpha\left[\frac{\partial^2 T'}{\partial x^2} + \frac{\partial^2 T'}{\partial y^2} + \frac{\partial^2 T'}{\partial z^2}\right], \end{aligned} \tag{22}$$

where the terms with the absolute value $|\vec{u}|$ in the above equations can be approximated as

$$\left|\vec{u}\right| = \sqrt{(\bar{u}+u')^2+(\bar{v}+v')^2+(w')^2} \approx \left|\bar{u}\right| = \bar{u}$$

for simplicity.

Following the method of order-of-magnitude analysis described by Hsu and Cheng [12], the terms $\partial u'/\partial x$ and $\partial^2 T'/\partial x^2$ in Eqs. (18) and (22) can be neglected. The pressure terms p' in Eqs. (19)–(21) are eliminated by cross differentiation and subtraction. Next, the resulting equations are differentiated with respect to z and the substitution of $\partial w'/\partial z = -\partial v'/\partial y$ from the continuity equation is employed to remove the terms involving the component w' and its derivatives. These operations will lead to the following three equations involving the disturbance quantities u', v' and T':

$$\left(1+\frac{\rho_\infty cK}{\mu}\bar{u}\right)\left(\frac{\partial^2 u'}{\partial z^2}+\frac{\partial^2 v'}{\partial x\partial y}\right)+\frac{\rho_\infty cK}{\mu}\frac{\partial \bar{u}}{\partial x}\frac{\partial v'}{\partial y} = \frac{\rho_\infty g\beta K\sin\varphi}{\mu}\frac{\partial^2 T'}{\partial z^2}, \tag{23}$$

$$\left(1+\frac{\rho_\infty cK}{\mu}\bar{u}\right)\left(\frac{\partial^2 v'}{\partial z^2}+\frac{\partial^2 v'}{\partial y^2}\right)+\frac{\rho_\infty cK}{\mu}\frac{\partial \bar{u}}{\partial y}\frac{\partial v'}{\partial y} = \frac{\rho_\infty g\beta K\cos\varphi}{\mu}\frac{\partial^2 T'}{\partial z^2}, \tag{24}$$

$$\lambda\frac{\partial T'}{\partial t}+\bar{u}\frac{\partial T'}{\partial x}+u'\frac{\partial T'}{\partial x}+\bar{v}\frac{\partial T'}{\partial y}+v'\frac{\partial \bar{T}}{\partial y} = \alpha\left[\frac{\partial^2 T'}{\partial y^2}+\frac{\partial^2 T'}{\partial z^2}\right]. \tag{25}$$

Next, by applying the non-parallel flow model which assumes that the amplitudes of the disturbances are functions of both x and y, the three-dimensional disturbance quantities are expressed as

$$\begin{aligned} u'(x,y,z,t) &= \tilde{u}(x,y)\cdot\exp[\mathrm{i}az+\sigma t+\gamma(x)],\\ v'(x,y,z,t) &= \tilde{v}(x,y)\cdot\exp[\mathrm{i}az+\sigma t+\gamma(x)],\\ T'(x,y,z,t) &= \tilde{T}(x,y)\cdot\exp[\mathrm{i}az+\sigma t+\gamma(x)], \end{aligned} \tag{26}$$

where a is the spanwise periodic wave number, σ is the temporal growth factor, and $\gamma(x)=\int\alpha_i(x)\mathrm{d}x$, with $\alpha_i(x)$ denoting the spatial growth factor which is a weak function of x. Substituting Eq. (26) into Eqs. (23)–(25) and setting $\sigma=\alpha_i=0$ for the stationary neutral stability condition yields

$$\left(1+\frac{\rho_\infty cK}{\mu}\bar{u}\right)\left(a^2\tilde{u}-\frac{\partial^2\tilde{v}}{\partial x\partial y}\right)-\frac{\rho_\infty cK}{\mu}\frac{\partial\bar{u}}{\partial x}\frac{\partial\tilde{v}}{\partial y} = \frac{\rho_\infty g\beta Ka^2}{\mu}\tilde{T}\sin\varphi, \tag{27}$$

$$\left(1+\frac{\rho_\infty cK}{\mu}\bar{u}\right)\left(a^2\tilde{v}-\frac{\partial^2\tilde{v}}{\partial y^2}\right)-\frac{\rho_\infty cK}{\mu}\frac{\partial\bar{u}}{\partial y}\frac{\partial\tilde{v}}{\partial y} = \frac{\rho_\infty g\beta Ka^2}{\mu}\tilde{T}\cos\varphi, \tag{28}$$

$$\bar{u}\frac{\partial\tilde{T}}{\partial x}+\tilde{u}\frac{\partial\bar{T}}{\partial x}+\bar{v}\frac{\partial\tilde{T}}{\partial y}+\tilde{v}\frac{\partial\bar{T}}{\partial y} = \alpha\left(\frac{\partial^2\tilde{T}}{\partial y^2}-a^2\tilde{T}\right), \tag{29}$$

with the boundary conditions

$$\tilde{u}=\tilde{v}=\tilde{T}=0 \text{ at } y=0 \text{ and } y\to\infty. \tag{30}$$

To simplify solutions of Eqs. (27)–(30), the first step is to eliminate $\tilde{u}$ by combining Eqs. (27) and (29), resulting in only two functions $\tilde{v}$ and $\tilde{T}$ in the equations. Next, by introducing the following dimensionless quantities

$$\begin{aligned} v^+(\xi,\eta) &= \frac{\tilde{v}}{5a\alpha(Ra_x/5)^{1/5}}, \quad \theta^+(\xi,\eta)=\frac{\tilde{T}}{T_\mathrm{w}-T_\infty}=\frac{\tilde{T}}{Ax^m},\\ k &= \frac{ax}{(Ra_x/5)^{1/5}}, \end{aligned} \tag{31}$$

Eqs. (27)–(30) can be transformed into the following system of dimensionless equations

$$a_1\mathrm{D}^2v^+ + a_2\mathrm{D}v^+ + a_3v^+ + a_4\theta^+ = 0, \tag{32}$$

$$b_1\mathrm{D}^2\theta^+ + b_2\mathrm{D}\theta^+ + b_3\theta^+ + b_4v^+ + b_5\mathrm{D}v^+ + b_6\mathrm{D}^2v^+ + b_7\frac{\partial}{\partial\xi}\mathrm{D}v^+ + b_8\frac{\partial}{\partial\xi}\mathrm{D}\theta^+ = 0, \tag{33}$$

with the boundary conditions

$$v^+=\theta^+=0, \text{ at } \eta=0 \text{ and } \eta\to\infty, \tag{34}$$

where D denotes partial differentiation with respect to η. The coefficients a_n and b_n, which are determined from the solutions of the basic flow, are given by

$$\begin{aligned} &a_1=\xi U, \quad a_2=Gf'', \quad a_3=-k^2\cdot a_1,\\ &a_4=k(Ra_x/5)^{1/5}\cos\varphi,\\ &b_1=1, \quad b_2=(m+3)f+(4-2m)\xi\frac{\partial f}{\partial\xi},\\ &b_3=-k^2-5mf'-5H\sin\varphi,\\ &b_4=-5k(Ra_x/5)^{1/5}\theta',\\ &b_5=-(2m+1+C)B, \quad b_6=-(m-2)\eta B,\\ &b_7=-(4-2m)\xi B, \quad b_8=-(4-2m)\xi f'. \end{aligned} \tag{35}$$

The expressions for B, C, H, G and U are given in Eq. (A.2).

Eqs. (32) and (33), along with the boundary conditions (34), constitute the mathematical system for the thermal instability problem under consideration. They are coupled parabolic partial differential equations, but

the boundary conditions as given are not sufficient to give an initial profile at a certain ξ_0 position. Therefore, a common "marching method" for parabolic differential equations cannot be employed to obtain the complete solution. Generally, two simple techniques can be employed to solve such a system of equations: the local similarity method and the local non-similarity method. In the local similarity method, in which the disturbance amplitude functions are assumed to have a weak dependence in the streamwise direction (i.e., $\partial/\partial\xi \ll \partial/\partial\eta$), the last two terms involving the derivative with respect to ξ in Eq. (33) are neglected, as was done by previous investigators. This is the quasi-parallel flow model approach. The system of partial differential Eqs. (32) and (33) can then be reduced to a set of linear ordinary differential equations whose solution can be easily obtained with the boundary conditions (34).

In the non-parallel flow model using the method of local non-similarity approximations, all the terms in Eqs. (32) and (33) are retained. This necessitates finding the equations for $\partial v^+/\partial\xi$ and $\partial\theta^+/\partial\xi$. Differentiation of Eqs. (32) and (33), as well as the boundary conditions (34), with respect to ξ will give two additional partial differential equations for $\partial v^+/\partial\xi$ and $\partial\theta^+/\partial\xi$, along with an additional set of the corresponding boundary conditions. To obtain the next higher order of equations for $\partial^2 v^+/\partial\xi^2$ and $\partial^2\theta^+/\partial\xi^2$, the differential equations and boundary conditions for $\partial v^+/\partial\xi$ and $\partial\theta^+/\partial\xi$ are differentiated again with respect to ξ. For the third-level of truncation, all the terms involving the third-order partial derivative with respect to ξ, $\partial^3 v^+/\partial\xi^3$ and $\partial^3\theta^+/\partial\xi^3$, are neglected in the subsidiary equations and boundary conditions. This operation will lead to the following system of equations and boundary conditions for v^+, θ^+, $\sigma = \partial v^+/\partial\xi$, $\omega = \partial\theta^+/\partial\xi$, $g = \partial\sigma/\partial\xi = \partial^2 v^+/\partial\xi^2$ and $h = \partial\omega/\partial\xi = \partial^2\theta^+/\partial\xi^2$:

$$
\begin{aligned}
&a_1 \mathrm{D}^2 v^+ + a_2 \mathrm{D}v^+ + a_3 v^+ + a_4\theta^+ = 0,\\
&b_1 \mathrm{D}^2\theta^+ + b_2 \mathrm{D}\theta^+ + b_3\theta^+ + b_4 v^+ + b_5 \mathrm{D}v^+ + b_6 \mathrm{D}^2 v^+\\
&\quad + b_7 \mathrm{D}\sigma + b_8 \mathrm{D}\omega = 0,\\
&c_1 \mathrm{D}^2\sigma + c_2 \mathrm{D}\sigma + c_3\sigma + c_4 \mathrm{D}^2 v^+ + c_5 \mathrm{D}v^+ + c_6 v^+\\
&\quad + c_7\omega + c_8\theta^+ = 0,\\
&d_1 \mathrm{D}^2\omega + d_2 \mathrm{D}\omega + d_3\omega + d_4 v^+ + d_5 \mathrm{D}v^+ + d_6 \mathrm{D}^2 v^+\\
&\quad + d_7\theta^+ + d_8 \mathrm{D}\theta^+ + d_9\sigma + d_{10} \mathrm{D}\sigma + d_{11} \mathrm{D}^2\sigma\\
&\quad + d_{12}h + d_{13} \mathrm{D}g = 0,\\
&e_1 \mathrm{D}^2 g + e_2 \mathrm{D}g + e_3 g + e_4 \mathrm{D}\sigma^2 + e_5 \mathrm{D}\sigma + e_6\sigma + e_7 \mathrm{D}^2 v^+\\
&\quad + e_8 \mathrm{D}v^+ + e_9 v^+ + e_{10}h + e_{11}\omega + e_{12}\theta^+ = 0,\\
&f_1 \mathrm{D}^2 h + f_2 \mathrm{D}h + f_3 h + f_4 g + f_5 \mathrm{D}g + f_6 \mathrm{D}^2 g + f_7\sigma\\
&\quad + f_8 \mathrm{D}\sigma + f_9 \mathrm{D}^2\sigma + f_{10}\omega + f_{11} \mathrm{D}\omega + f_{12} v^+ + f_{13} \mathrm{D}v^+\\
&\quad + f_{14} \mathrm{D}^2 v^+ + f_{15}\theta^+ + f_{16} \mathrm{D}\theta^+ = 0,
\end{aligned}
\tag{36}
$$

with the boundary conditions

$$
v^+ = \theta^+ = \sigma = \omega = g = h = 0 \text{ at } \eta = 0 \text{ and } \eta \to \infty. \tag{37}
$$

In Eq. (36), the coefficients a_n and b_n are as given in Eq. (35), and the coefficients c_n, d_n, e_n, and f_n are shown in Eq. (A.1).

The set of coupled linear ordinary differential Eq. (36), along with the homogeneous boundary conditions (37), forms a closed form of mathematical system of equations for the instability problem, which constitutes an eigenvalue problem of the form

$$
E(Ra_x, k; \varphi, m, Fr, \xi) = 0. \tag{38}
$$

In determining the neutral stability curve for given values of wall temperature exponent m, inclination angle φ, Forchheimer number Fr, and local Darcy number Da_x or non-similarity parameter ξ, the value of wave number k satisfying Eq. (38) is sought as the eigenvalue for a prescribed value of Rayleigh number Ra_x.

3. Numerical method of solutions

The system of Eqs. (13)–(15) for the basic flow and thermal fields are solved by an efficient and accurate implicit finite-difference method which is similar to that described by Cebeci and Bradshaw [18]. Along with a cubic spline interpolation procedure, the basic flow solutions provide the basic flow quantities f, f', f'', θ, θ', and their partial derivatives with respect to ξ that are required in the stability computations.

The stability problem, which is described by the system of Eqs. (36) and (37), can also be solved with an implicit finite-difference method similar to that for the basic flow. Here it suffices to mention the highlights of the eigenvalue problem. With a pre-assigned value of the non-similarity parameter $\xi = 1/[Da_x(Ra_x/5)^{2/5}]$ and Rayleigh number Ra_x, the basic flow solution is first obtained for fixed values of Forchheimer number Fr, inclination angle φ and wall temperature variation exponent m. Next, with a guessed value of wave number k as the eigenvalue and a non-zero value boundary condition $Dv^+(\xi, 0) = 1$ as the normalizing condition, the eigenvalue problem is solved. The guessed eigenvalue k is then determined by the Newton–Raphson differential-correction iterative scheme until all the boundary conditions at the wall ($\eta = 0$) are satisfied within a certain specified tolerance (with $\epsilon = 1 \times \mathrm{e}^{-6}$). This yields a converged value of k for given values of m, φ, Fr, Ra_x and ξ.

In the numerical calculations, a step size of $\Delta\xi = 0.01$ was found to give accurate results for both the basic flow and the disturbance flow. It is worthwhile to note that a larger step size $\Delta\xi$ could not be used in the numerical solutions of the basic flow even when the end point ξ is very large, which is often employed to cut down the

computation time in other cases. This is due to the special form of the basic flow equations, which is singular when $\xi = 0$. An initial profile at a very small starting point, such as $\xi_0 = 0.01$, is obtained based on the local similarity method. Then the "marching method" for parabolic partial differential equations is used to obtain solutions for the basic flow quantities. The accuracy of the basic flow solutions is verified through a comparison of the $\theta'(\xi, 0)$ value with that for the case of natural convection along a horizontal flat plate, which has similarity solutions [11]. In the η direction, $\Delta\eta = 0.01$ and $\eta_\infty = 10.0$ were found to be sufficient to give accurate results for both the basic flow and stability calculations. However, larger η_∞ values were needed and used when ξ is larger than 50.

4. Results and discussion

Representative numerical results are presented for the cases of $m = 0$, which corresponds to the isothermal surface condition (UWT), and $m = 1/3$, which corresponds approximately to the constant wall heat flux condition (UHF). The latter condition results from the expression

$$\begin{aligned} q_w(x) &= -k(\partial\bar{T}/\partial y)_{y=0} \\ &= -k(T_w(x) - T_\infty)\theta'(\xi, 0)(Ra_x/5)^{1/5}/x \\ &\propto x^{2(3m-1)/5}\theta'(\xi, 0). \end{aligned}$$

The velocity and temperature distributions across the boundary layer as well as the local Nusselt number $Nu_x(Ra_x/5)^{-1/5}$ or the local surface heat transfer rate for the basic flow are not shown. They are similar to those shown in Chang and Jang [16]. It suffices to mention that the inertia effect (Fr) reduces the surface heat transfer rate. To verify the validity of the present solutions, the present results are compared with those of Jang and Chang [14] for the case of pure Darcy flow. The comparison shows that an excellent agreement exists between the two separate calculations.

The neutral stability curves for different values of Forchheimer number Fr(0, 10 and 20) for $\xi = 10$, $m = 0$, and inclination angles of 0°, 30°, and 50° are shown, respectively, in Figs. 2–4. Results from solutions based on the parallel flow model and the non-parallel flow model are included for comparisons. The flow is stable in the region below a neutral stability curve and is unstable in the region above the curve. The minimum Rayleigh number Ra_x on a neutral stability curve is the critical Rayleigh number, Ra_x^*, with a corresponding critical wave number k^*. The flow is therefore stable if the Rayleigh number Ra_x is smaller than the critical Rayleigh number Ra_x^* and is unstable when Ra_x is larger than Ra_x^*.

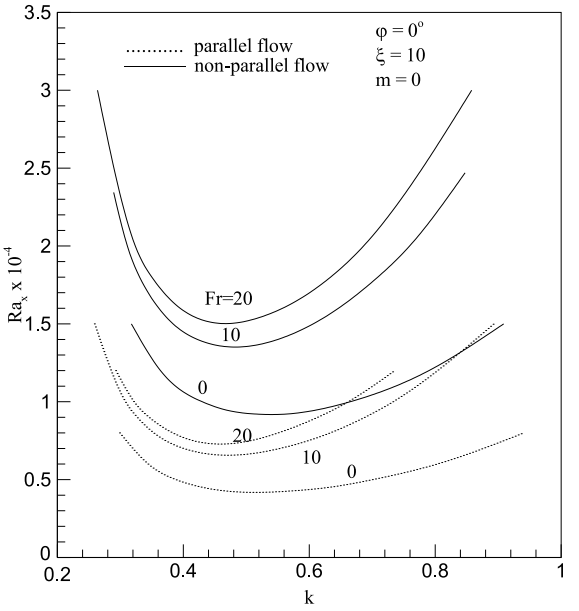

Fig. 2. Neutral stability curves for different values of Fr ($\varphi = 0°, \xi = 10, m = 0$).

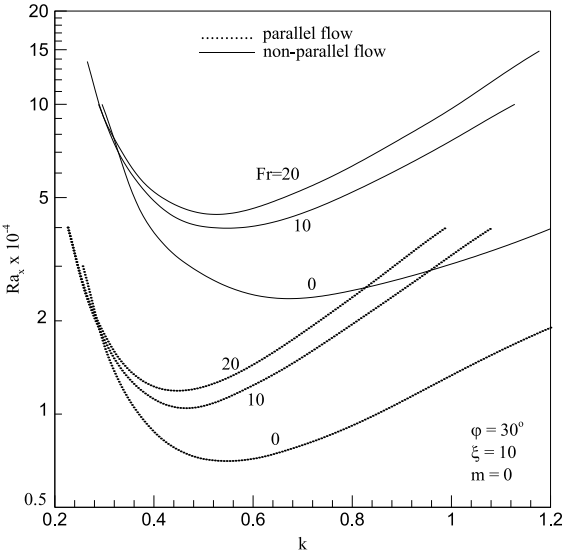

Fig. 3. Neutral stability curves for different values of Fr ($\varphi = 30°, \xi = 10, m = 0$).

From Figs. 2–4, it can be seen that a large discrepancy in the results exists between the parallel flow model and the non-parallel flow model. The critical Rayleigh numbers, Ra_x^*, predicted by the non-parallel flow model are much higher than those by the parallel flow model, which means that the assumption of a weak dependence of the disturbance amplitude functions on the stream-

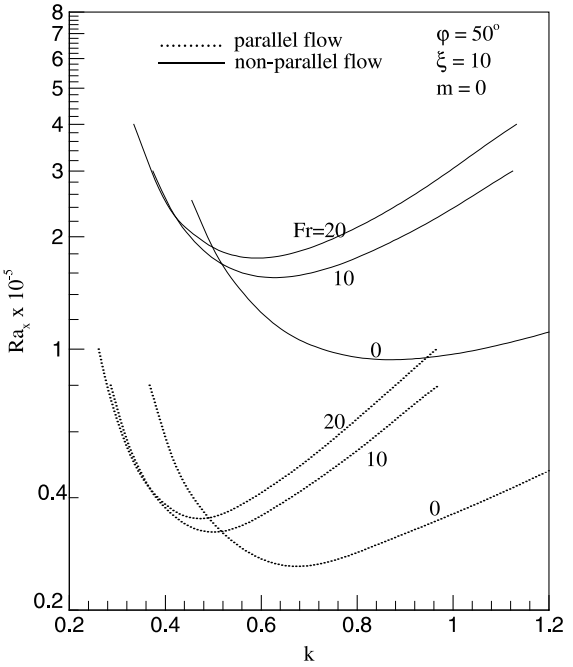

Fig. 4. Neutral stability curves for different values of Fr ($\varphi = 50°, \xi = 10, m = 0$).

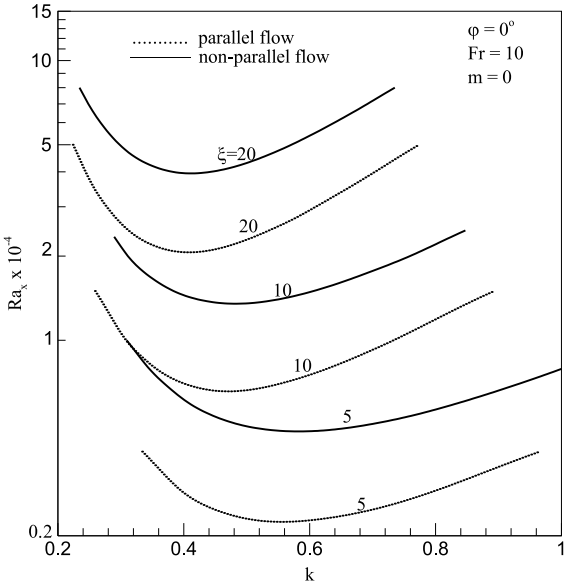

Fig. 5. Neutral stability curves for different values of ξ ($\varphi = 0°, Fr = 10, m = 0$).

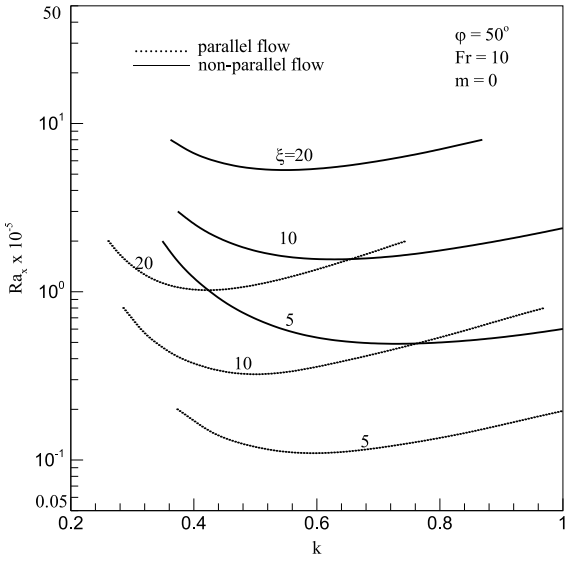

Fig. 6. Neutral stability curves for different values of ξ ($\varphi = 50°, Fr = 10, m = 0$).

wise coordinate (i.e., $\partial/\partial\xi \ll \partial/\partial\eta$) in the instability analysis based on the parallel flow model is not valid, because the ξ-dependent disturbance terms neglected in the parallel flow model have a great stabilizing effect. Figs. 2–4 also show that the neutral stability curve for a larger Fr number lies above the curve with a smaller Fr number, which states that the inertia effect contributes to a more stable flow. This conclusion is contrary to that reached by Chang and Jang [16], but agrees with that drawn by Lee et al. [17], because the former made a wrong interpretation of inertia terms in the disturbance equations.

Figs. 5 and 6 show, respectively, the neutral stability curves for the horizontal case ($\varphi = 0°$) and for the case of an inclined plate ($\varphi = 50°$) at different values of ξ (5, 10, and 20) for $Fr = 10$ and $m = 0$. It is seen that the flow becomes more stable with a larger value of ξ, which means that a weaker convective flow (i.e., smaller Ra_x or ΔT) makes the flow more stable, or flow in a porous medium with a lower permeability K is less susceptible to the vortex mode of instability.

Fig. 7 shows a comparison of the neutral stability curves for $Fr = 0$, 10, 20 at $\xi = 10$ between the values of $m = 0$ and $m = 1/3$ for an inclined plate ($\varphi = 30°$). To conserve space, similar neutral stability curves are not shown for the horizontal plate ($\varphi = 0°$) and other inclination angles. This figure shows that $m = 0$ (i.e., constant wall temperature case) gives rise to a more unstable flow than $m = 1/3$, because $m = 0$ corresponds to a step change in the wall temperature, which induces a heating condition that makes the flow more susceptible to thermal instability than $m = 1/3$ and other values of m which have a slower increase in the wall temperature along the x-coordinate. It also shows that $m = 1/3$ gives larger critical Rayleigh numbers, which means a more stable flow. This is due to the fact that the streamwise driving force (i.e., the terms $\bar{u}(\partial\tilde{T}/\partial x)$ and $\tilde{u}(\partial\bar{T}/\partial x)$ in

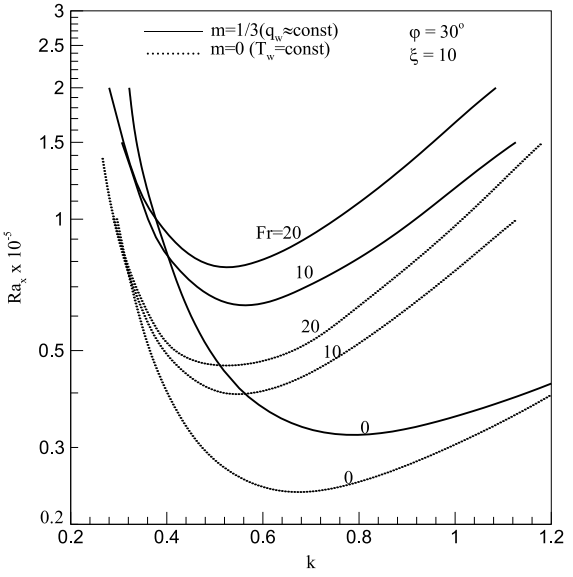

Fig. 7. Comparisons of neutral stability curves for different values of m and Fr ($\varphi = 30°, \xi = 10$).

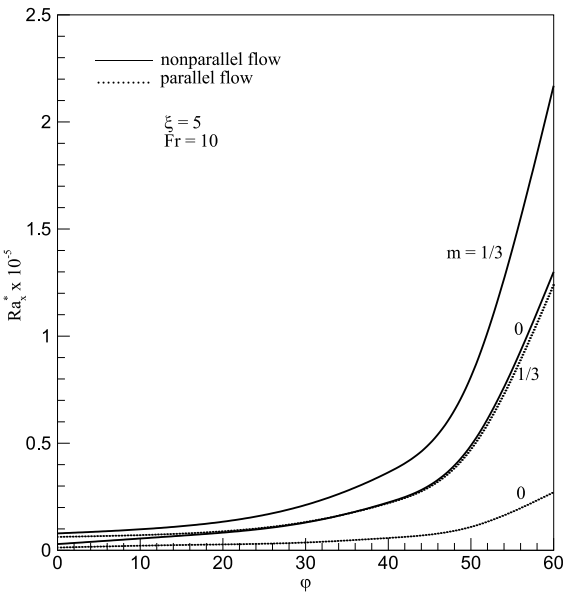

Fig. 9. Critical Rayleigh number Ra_x^* for different inclination angles ($\xi = 5, Fr = 10, m = 0$ and 1/3).

Eq. (29)) increases as m increases from 0 and thus reduces the relative effect of the normal component of the buoyancy force.

Fig. 8 shows the neutral stability curves for various inclination angles φ (0°, 30°, 40° and 50°) at given values of $\xi = 5$ and $Fr = 10$ for $m = 0$. Fig. 9 shows the variation of critical Rayleigh number as a function of inclination angle φ for $m = 0$ and 1/3. These two figures clearly show that the flow becomes more stable with an increase in the inclination angle from the horizontal. It should be noted that the flow becomes absolutely stable to the vortex mode of instability when the plate is in the vertical orientation ($\varphi = 90°$), because there is no buoyancy component normal to the plate under this condition. A comparison between results from the parallel flow model and non-parallel flow model is also presented in Figs. 8 and 9, which reveal again that the parallel flow model under-predicts the onset of vortex instability as compared with the non-parallel flow model.

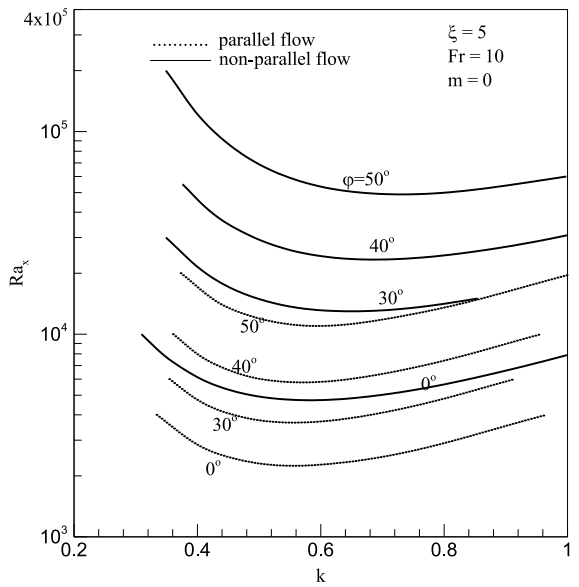

Fig. 8. Neutral stability curves for different inclination angles ($\xi = 5, Fr = 10, m = 0$).

A comparison of the critical Rayleigh numbers, Ra_x^*, as a function of ξ is illustrated in Fig. 10 for flow along an inclined plate ($\varphi = 50°$) with $m = 0$ for various values of the inertia effect Fr. A similar comparison of the critical Rayleigh numbers as a function of Fr for various ξ values is shown in Fig. 11. It can be seen from Figs. 10 and 11 that the critical Rayleigh numbers Ra_x^* from the parallel flow model are much lower than those from the non-parallel flow model. A comparison between the present results and those of Lee et al. [17] is also made in Fig. 10. To facilitate such a comparison, a transformation between the definitions of the different variables and parameters between the two are given here

$$\overline{Gr} = Ra_x \frac{cx}{Pr} Da_x^2 \sin\varphi = \frac{(Ra_x/5)^{1/5}}{\xi^2} Fr^{1/(2-m)} \xi^{5/(4-2m)} \sin\varphi,$$

$$\overline{Ra_x} = Ra_x Da_x \sin\varphi = \frac{5}{\xi} (Ra_x/5)^{3/5} \sin\varphi, \tag{39}$$

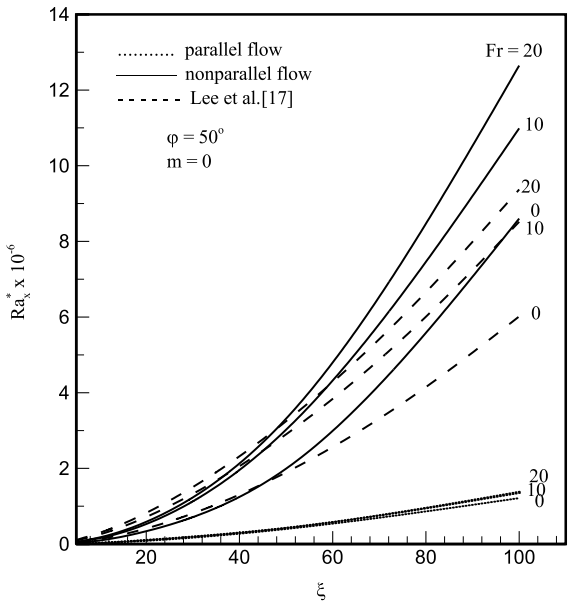

Fig. 10. Critical Rayleigh number Ra_x^* vs ξ for different values of Fr ($\varphi = 50°, m = 0$).

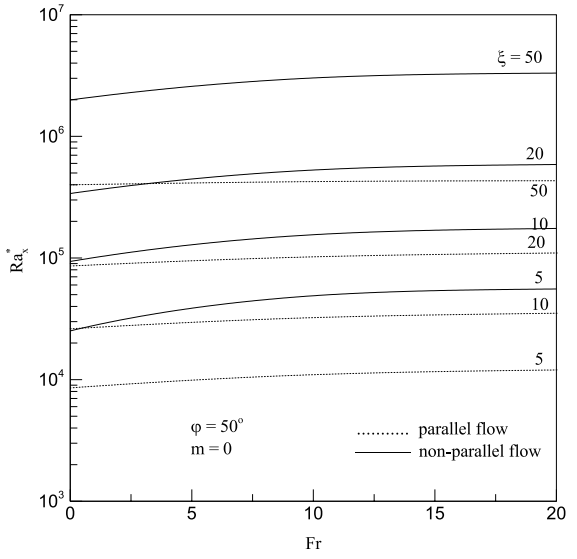

Fig. 11. Critical Rayleigh number Ra_x^* vs Fr for different values of ξ ($\varphi = 50°, m = 0$).

where $\overline{Gr}$ and $\overline{Ra_x}$ are parameters defined in [17]. It is noted that only results from the non-parallel flow model in the present computations can be compared with the results of Lee et al. [17]. This comparison shows that for natural convection on inclined plates (Fig. 10), whether the inertia effect is included ($Fr \neq 0$) or not ($Fr = 0$), the present predictions by the non-parallel flow model give a higher (lower) critical value of Ra_x^* for a larger (smaller) value of ξ than those by Lee et al. [17]. This discrepancy is likely due to their solution methods which neglected the higher order ξ-dependent terms.

A final note is in order here. Because of a total lack of experimental data in the literature that could be used for comparisons, it cannot be conclusively verified that, for flow in porous media, the non-parallel flow model provides more accurate thermal instability results than the parallel flow model, as was verified by Lee et al. [8,9] for clear fluids in a comparison between their analytical results and available experimental data. However, it is expected that the conclusion drawn from clear fluids should apply to fluid-saturated porous media as well.

5. Conclusions

The inertia effect on the vortex instability of natural convection flow over horizontal and inclined flat plates embedded in a fluid-saturated porous medium has been examined using the Forchheimer non-Darcy model. The non-parallel flow model is employed in the instability analysis. The transformed dimensionless governing equations for the amplitude functions of the disturbance flow are reduced to a system of homogeneous linear ordinary differential equations with homogeneous boundary conditions by the local non-similarity method. The resulting eigenvalue problem is solved by an implicit finite-difference method. The major findings from the present study are: (1) the present study can predict the onset of vortex instability for all angles of inclination ($0 \leqslant \varphi < 90°$) relative to the horizontal; (2) the non-parallel flow model predicts a higher critical Rayleigh number than the parallel flow model; (3) the flow becomes more stable to the vortex mode of instability as the angle of inclination φ increases; (4) the flow becomes more stable with an increasing value of the exponent m of the wall temperature; (5) the inertia effect has a stabilizing effect on the instability of the flow and (6) the non-parallel flow model is a better model to use in the flow instability analysis than the parallel flow model.

Appendix A

The coefficients c_n, d_n, e_n, and f_n appearing in Eq. (36) are

$$c_1 = a_1, \quad c_2 = a_2, \quad c_3 = a_3, \quad c_4 = U + \xi \frac{\partial U}{\partial \xi},$$

$$c_5 = G \frac{\partial f''}{\partial \xi} + \frac{\partial G}{\partial \xi} f'',$$

$$c_6 = -\frac{k^2}{\xi} a_1 - k^2 c_4, \quad c_7 = a_4,$$

$$c_8 = \frac{5}{4 - 2m} \frac{k(Ra_x/5)^{1/5}}{\xi} \cos \varphi,$$

$$
\begin{aligned}
&d_1 = b_1, \quad d_2 = b_2, \quad d_3 = b_3 - (4-2m)\left(f' + \xi\frac{\partial f'}{\partial \xi}\right),\\
&d_4 = -\frac{k(Ra_x/5)^{1/5}}{\xi}\left(\frac{5}{4-2m}\theta' + \xi\frac{\partial \theta'}{\partial \xi}\right),\\
&d_5 = -B\frac{\partial C}{\partial \xi} - (2m+1+C)\frac{\partial B}{\partial \xi}, \quad d_6 = -(m-2)\eta\frac{\partial B}{\partial \xi},\\
&d_7 = -5m\frac{\partial f'}{\partial \xi} - \frac{k^2}{\xi} - 5\frac{\partial H}{\partial \xi}\sin\varphi,\\
&d_8 = (7-m)\frac{\partial f}{\partial \xi} + (4-2m)\xi\frac{\partial^2 f}{\partial \xi^2},\\
&d_9 = b_4, \quad d_{10} = b_5 - (4-2m)\left(B + \xi\frac{\partial B}{\partial \xi}\right),\\
&d_{11} = b_6, \quad d_{12} = b_8, \quad d_{13} = b_7,\\
&e_1 = c_1, \quad e_2 = c_2, \quad e_3 = c_3, \quad e_4 = 2c_4,\\
&e_5 = 2c_5, \quad e_6 = 2c_6,\\
&e_7 = 2\frac{\partial U}{\partial \xi} + \xi\frac{\partial^2 U}{\partial \xi^2}, \quad e_8 = 2\frac{\partial G}{\partial \xi}\frac{\partial f''}{\partial \xi} + f''\frac{\partial^2 G}{\partial \xi^2} + G\frac{\partial^2 f''}{\partial \xi^2},\\
&e_9 = -\frac{k^2}{\xi}(2c_4 + \xi\cdot e_7), \quad e_{10} = c_7, \quad e_{11} = 2c_8,\\
&e_{12} = \frac{5(1+2m)}{(4-2m)^2}\frac{k(Ra_x/5)^{1/5}}{\xi^2}\cos\varphi,\\
&f_1 = d_1, \quad f_2 = d_2,\\
&f_3 = d_3 - (4-2m)\left(f' + \xi\frac{\partial f'}{\partial \xi}\right), \quad f_4 = d_9,\\
&f_5 = d_{10} - (4-2m)\left(B + \xi\frac{\partial B}{\partial \xi}\right),\\
&f_6 = d_{11}, \quad f_7 = 2d_4,\\
&f_8 = 2d_5 - (4-2m)\left(2\frac{\partial B}{\partial \xi} + \xi\frac{\partial^2 B}{\partial \xi^2}\right), \quad f_9 = 2d_6,\\
&f_{10} = 2d_7 - (4-2m)\left(2\frac{\partial f'}{\partial \xi} + \xi\frac{\partial^2 f'}{\partial \xi^2}\right), \quad f_{11} = 2d_8,\\
&f_{12} = -\frac{5k(Ra_x/5)^{1/5}}{\xi^2}\left(\frac{5(1+2m)}{(4-2m)^2}\theta' + \frac{5}{2-m}\xi\frac{\partial \theta'}{\partial \xi} + \xi^2\frac{\partial^2 \theta'}{\partial \xi^2}\right),\\
&f_{13} = -2\frac{\partial C}{\partial \xi}\frac{\partial B}{\partial \xi} - B\frac{\partial^2 C}{\partial \xi^2} - (2m+1+C)\frac{\partial^2 B}{\partial \xi^2},\\
&f_{14} = -(m-2)\eta\frac{\partial^2 B}{\partial \xi^2},\\
&f_{15} = -5m\frac{\partial^2 f'}{\partial \xi^2} + 5\frac{\partial^2 H}{\partial \xi^2}\sin\varphi,\\
&f_{16} = (11-3m)\frac{\partial^2 f}{\partial \xi^2} + (4-2m)\xi\frac{\partial^3 f}{\partial \xi^3}.
\end{aligned}
\tag{A.1}
$$

The expressions for B, C, E, F, G, H, U and their respective ξ-derivatives are given by

$$
\begin{aligned}
&B = \frac{F}{k(Ra_x/5)^{1/5}},\\
&\frac{\partial B}{\partial \xi} = \frac{\partial F/\partial \xi}{k(Ra_x/5)^{1/5}} - \frac{5}{4-2m}\frac{F}{\xi k(Ra_x/5)^{1/5}},\\
&\frac{\partial^2 B}{\partial \xi^2} = \frac{\partial^2 F/\partial \xi^2}{k(Ra_x/5)^{1/5}} - \frac{5}{4-2m}\frac{\partial F/\partial \xi}{\xi k(Ra_x/5)^{1/5}}\\
&\qquad - \frac{5}{4-2m}\left(\frac{\partial F/\partial \xi}{\xi k(Ra_x/5)^{1/5}} - \frac{9-2m}{4-2m}\frac{F}{\xi^2 k(Ra_x/5)^{1/5}}\right),\\
&C = Fr^{1/(2-m)}\xi^{(1+2m)/(4-2m)}E/U,\\
&\frac{\partial C}{\partial \xi} = \frac{G}{\xi U}\frac{\partial E}{\partial \xi} + \frac{E}{U^2}\left(\frac{1+2m}{4-2m}\frac{G}{\xi^2}U - \frac{G}{\xi}\frac{\partial U}{\partial \xi}\right),\\
&\frac{\partial^2 C}{\partial \xi^2} = \frac{G}{\xi U}\frac{\partial^2 E}{\partial \xi^2} + \frac{\partial E}{\partial \xi}\frac{1}{U^2}\left(\frac{1+2m}{4-2m}\frac{G}{\xi^2}U - \frac{G}{\xi}\frac{\partial U}{\partial \xi}\right)\\
&\qquad + \frac{G}{\xi^2 U^2}\frac{\partial E}{\partial \xi}\left(\frac{1+2m}{4-2m}U - \xi\frac{\partial U}{\partial \xi}\right)\\
&\qquad + \frac{4m-3}{4-2m}E\frac{G}{\xi^3}\left(\frac{1+2m}{4-2m}\frac{1}{U} - \frac{\xi}{U^2}\frac{\partial U}{\partial \xi}\right)\\
&\qquad - E\frac{G}{\xi^2}\left(\frac{5}{4-2m}\frac{1}{U^2}\frac{\partial U}{\partial \xi} + \frac{\xi}{U^2}\frac{\partial^2 U}{\partial \xi^2} - \frac{2\xi}{U^3}\frac{\partial U}{\partial \xi}\frac{\partial U}{\partial \xi}\right),\\
&E = (2m+1)f' + (m-2)\eta f'' + (4-2m)\xi\frac{\partial f'}{\partial \xi},\\
&\frac{\partial E}{\partial \xi} = 5\frac{\partial f'}{\partial \xi} + (m-2)\eta\frac{\partial f''}{\partial \xi} + (4-2m)\xi\frac{\partial^2 f'}{\partial \xi^2},\\
&\frac{\partial^2 E}{\partial \xi^2} = (9-2m)\frac{\partial^2 f'}{\partial \xi^2} + (m-2)\eta\frac{\partial^2 f''}{\partial \xi^2} + (4-2m)\xi\frac{\partial^3 f'}{\partial \xi^3},
\end{aligned}
\tag{A.2}
$$

$$
\begin{aligned}
&F = m\theta + \frac{m-2}{5}\eta\theta' + \frac{4-2m}{5}\xi\frac{\partial \theta}{\partial \xi},\\
&\frac{\partial F}{\partial \xi} = \frac{3m+4}{5}\frac{\partial \theta}{\partial \xi} + \frac{4-2m}{5}\xi\frac{\partial^2 \theta}{\partial \xi^2} + \frac{m-2}{5}\eta\frac{\partial \theta'}{\partial \xi},\\
&\frac{\partial^2 F}{\partial \xi^2} = \frac{m+8}{5}\frac{\partial^2 \theta}{\partial \xi^2} + \frac{m-2}{5}\eta\frac{\partial^2 \theta'}{\partial \xi^2} + \frac{4-2m}{5}\xi\frac{\partial^3 \theta}{\partial \xi^3},\\
&G = Fr^{1/(2-m)}\xi^{5/(4-2m)}, \quad \frac{\partial G}{\partial \xi} = \frac{5}{4-2m}\frac{G}{\xi},\\
&\frac{\partial^2 G}{\partial \xi^2} = \frac{5(1+2m)}{(4-2m)^2}\frac{G}{\xi^2},\\
&H = \frac{(Ra_x/5)^{1/5}}{\xi}\frac{F}{U},\\
&\frac{\partial H}{\partial \xi} = \frac{3m-1}{4-2m}\frac{H}{\xi} + \frac{(Ra_x/5)^{1/5}}{\xi U}\left(\frac{\partial F}{\partial \xi} - \frac{F}{U}\frac{\partial U}{\partial \xi}\right),
\end{aligned}
$$

$$\frac{\partial^2 H}{\partial \xi^2} = \frac{5(m-1)(3m-1)}{(4-2m)^2}\frac{H}{\xi^2} + \frac{3m-1}{2-m}\frac{(Ra_x/5)^{1/5}}{\xi^2 U} \times \left(\frac{\partial F}{\partial \xi} - \frac{F}{U}\frac{\partial U}{\partial \xi}\right) + \frac{(Ra_x/5)^{1/5}}{\xi U} \times \left(\frac{\partial^2 F}{\partial \xi^2} - \frac{2}{U}\frac{\partial F}{\partial \xi} - \frac{F}{U}\frac{\partial^2 U}{\partial \xi^2} + \frac{2F}{U^2}\frac{\partial U}{\partial \xi}\right),$$

$$U = 1 + \frac{\rho_\infty c K}{\mu}\bar{u} = 1 + \frac{5cx}{\xi} f' = 1 + Fr^{1/(2-m)}\xi^{(1+2m)/(4-2m)} f',$$

$$\frac{\partial U}{\partial \xi} = Fr^{1/(2-m)}\xi^{(1+2m)/(4-2m)}\left(\frac{1+2m}{4-2m}\frac{f'}{\xi} + \frac{\partial f'}{\partial \xi}\right),$$

$$\frac{\partial^2 U}{\partial \xi^2} = Fr^{1/(2-m)}\xi^{(6m-7)/(4-2m)}\left(\frac{(1+2m)(4m-3)}{(4-2m)^2} f' + \frac{1+2m}{2-m}\xi\frac{\partial f'}{\partial \xi} + \xi^2\frac{\partial^2 f'}{\partial \xi^2}\right).$$

References

[1] E.M. Sparrow, R.B. Husar, Longitudinal vortices in natural convection flow on inclined plates, J. Fluid Mech. 37 (1969) 251–255.

[2] J.R. Lloyd, E.M. Sparrow, On the instability of natural convection flow on inclined plates, J. Fluid Mech. 42 (1970) 465–470.

[3] G.J. Hwang, K.C. Cheng, Thermal instability of laminar natural convection flow on inclined isothermal plates, Can. J. Chem. Eng. 51 (1973) 659–666.

[4] S.E. Haaland, E.M. Sparrow, Vortex instability of natural convection flow on inclined surfaces, Int. J. Heat Mass Transfer 16 (1973) 2355–2367.

[5] T.S. Chen, K.L. Tzuoo, Vortex instability of free convection flow over horizontal and inclined surfaces, J. Heat Transfer 104 (1982) 637–643.

[6] H.C. Tien, T.S. Chen, B.F. Armaly, Vortex instability of natural convection flow over horizontal and inclined plates with uniform surface heat flux, Numerical Heat Transfer 9 (1986) 697–713.

[7] H.R. Lee, T.S. Chen, B.F. Armaly, Nonparallel thermal instability of forced convection flow over a heated nonisothermal horizontal flat plate, Int. J. Heat Mass Transfer 33 (1990) 2019–2028.

[8] H.R. Lee, T.S. Chen, B.F. Armaly, Nonparallel vortex instability of natural convection flow over a nonisothermal horizontal flat plate, Int. J. Heat Mass Transfer 34 (1991) 305–313.

[9] H.R. Lee, T.S. Chen, B.F. Armaly, Nonparallel thermal instability of natural convection flow on nonisothermal inclined flat plates, Int. J. Heat Mass Transfer 35 (1992) 207–220.

[10] H.R. Lee, T.S. Chen, B.F. Armaly, Nonparallel thermal instability of mixed convection flow on nonisothermal horizontal and inclined flat plates, Int. J. Heat Mass Transfer 35 (1992) 1913–1925.

[11] C.T. Hsu, P. Cheng, G.M. Homsy, Instability of free convection flow over a horizontal impermeable surface in a porous medium, Int. J. Heat Mass Transfer 21 (1978) 1221–1228.

[12] C.T. Hsu, P. Cheng, Vortex instability in buoyancy-induced flow over inclined heated surfaces in porous media, J. Heat Transfer 101 (1979) 660–665.

[13] C.T. Hsu, P. Cheng, The onset of longitudinal vortices in mixed convective flow over an inclined surface in a porous medium, J. Heat Transfer 102 (1980) 544–549.

[14] J.Y. Jang, W.J. Chang, Vortex instability of buoyancy-induced inclined boundary-layer flow in a saturated porous medium, Int. J. Heat Mass Transfer 31 (1988) 759–767.

[15] J.Y. Jang, K.N. Lie, Vortex instability of mixed convection flow over horizontal and inclined surfaces in a porous medium, Int. J. Heat Mass Transfer 35 (1992) 2077–2085.

[16] W.J. Chang, J.Y. Jang, Inertia effects on vortex instability of a horizontal natural convection flow in a saturated porous medium, Int. J. Heat Mass Transfer 32 (1989) 541–550.

[17] D.H. Lee, D.Y. Yoon, C.K. Choi, The onset of vortex instability in laminar natural convection flow over an inclined plate embedded in a porous medium, Int. J. Heat Mass Transfer 43 (2000) 2895–2908.

[18] T. Cebeci, P. Bradshaw, Physical and Computational Aspects of Convective Heat Transfer, Springer, New York, 1984 (Chapter 13).